Cell Reports

Report

Work Done by Titin Protein Folding Assists Muscle Contraction

Graphical Abstract

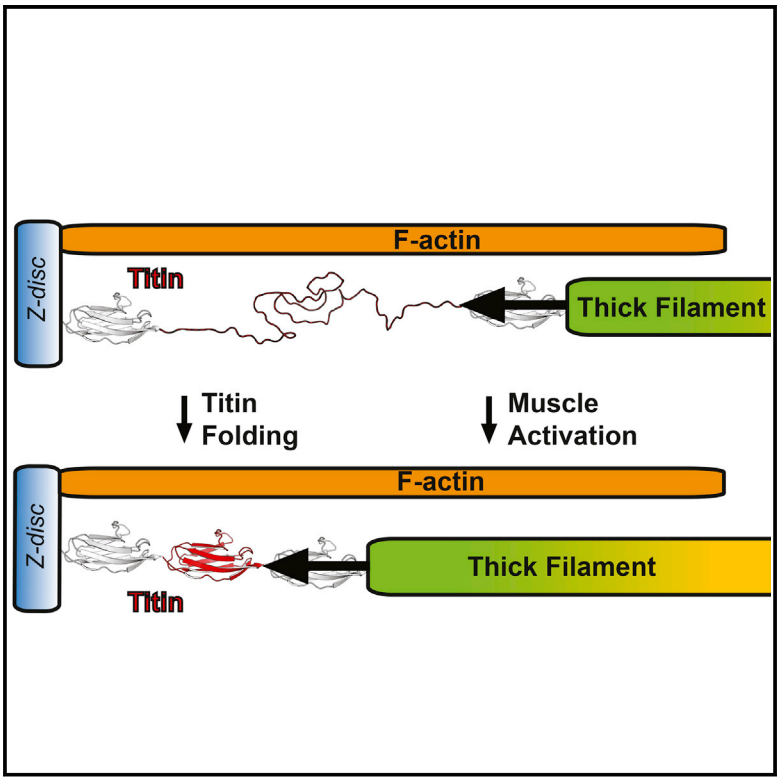

Authors

Jaime Andrés Rivas-Pardo, Edward C. Eckels, Ionel Popa, Pallav Kosuri, Wolfgang A. Linke, Julio M. Fernández

Correspondence

wolfgang.linke@rub.de (W.A.L.), jfernandez@columbia.edu (J.M.F.)

In Brief

Titin, the largest protein in the human body, is responsible for muscle elasticity, while myosin motors are thought to provide the sole source of contractile energy. Here, we find that titin unfolding occurs at forces below 10 pN and that subsequent refolding can produce substantial amounts of work that assist in muscle contraction.

Highlights

- Titin Ig domains unfold and refold continuously at physiological sarcomere lengths
- Refolding of titin domains generates mechanical work that assists muscle contraction
- Titin and myosin motors operate as an inextricable molecular system in muscle

Rivas-Pardo et al., 2016, Cell Reports *14*, 1339–1347
February 16, 2016
http://dx.doi.org/10.1016/j.celrep.2016.01.025

CellPress

Cell Reports
Report

Work Done by Titin Protein Folding Assists Muscle Contraction

Jaime Andrés Rivas-Pardo,[1,4] Edward C. Eckels,[1,2,4] Ionel Popa,[1] Pallav Kosuri,[1] Wolfgang A. Linke,[3,*] and Julio M. Fernández[1,*]
[1]Department of Biological Sciences, Columbia University, New York, NY 10027, USA
[2]Integated Program in Cellular, Molecular, and Biomedical Studies, Columbia University Medical Center, New York, NY 10032, USA
[3]Department of Cardiovascular Physiology, Ruhr University Bochum, 44780 Bochum, Germany
[4]Co-first author
*Correspondence: wolfgang.linke@rub.de (W.A.L.), jfernandez@columbia.edu (J.M.F.)
http://dx.doi.org/10.1016/j.celrep.2016.01.025

SUMMARY

Current theories of muscle contraction propose that the power stroke of a myosin motor is the sole source of mechanical energy driving the sliding filaments of a contracting muscle. These models exclude titin, the largest protein in the human body, which determines the passive elasticity of muscles. Here, we show that stepwise unfolding/folding of titin immunoglobulin (Ig) domains occurs in the elastic I band region of intact myofibrils at physiological sarcomere lengths and forces of 6–8 pN. We use single-molecule techniques to demonstrate that unfolded titin Ig domains undergo a spontaneous stepwise folding contraction at forces below 10 pN, delivering up to 105 zJ of additional contractile energy, which is larger than the mechanical energy delivered by the power stroke of a myosin motor. Thus, it appears inescapable that folding of titin Ig domains is an important, but as yet unrecognized, contributor to the force generated by a contracting muscle.

INTRODUCTION

The sliding filament hypothesis explains muscle contraction as resulting solely from the force generated by ATP-driven myosin motors that form reversible cross-bridges with actin filaments and generate force through a rotation of the myosin head: the power stroke (Huxley and Simmons, 1971). In these models, ATP hydrolysis stores elastic energy in the compliance of the cross-bridges themselves, delivering >38 zJ of contractile energy with each shortening step (Finer et al., 1994; Piazzesi et al., 2007). However, recent work has shown that only small amounts of elastic energy can be stored in the cross-bridges themselves (~5 zJ) (Piazzesi et al., 2014). Where does the returning elastic energy of a contracting muscle comes from? Remarkably, none of these studies considers the largest human protein found thus far: titin. Titin, the giant tandem modular protein anchored to myosin and the Z-disc in muscle sarcomeres (Figure 1A), is responsible for the passive elasticity of striated muscle tissue (Granzier and Labeit, 2002; Linke and Fernandez, 2002). Although titin has now been recognized as the third filament of muscle, its role is largely viewed as that of a passive spring that provides elastic recoil in relaxed sarcomeres without playing a role during active muscle contraction.

Force spectroscopy studies have uncovered the basic elements of how titin proteins respond to a stretching force; domains unfold and refold in a time- and force-dependent manner, while any unfolded polypeptide simply follows the laws of polymer elasticity (Kellermayer et al., 1997; Rief et al., 1997; Tskhovrebova et al., 1997). A significant discovery was the finding that unfolded proteins could actively collapse and refold while under force, thereby generating positive mechanical work (Fernandez and Li, 2004). However, domain unfolding/refolding of titin has been thought not to take place in intact muscle tissue and only operates as a safety mechanism to limit high forces in the sarcomere (Li et al., 2002; Tskhovrebova and Trinick, 2003). Therefore, the folding of titin domains has not been considered as a plausible mechanism for delivering elastic energy in conjunction with the cycling myosin motors during muscle contraction.

Here, we directly measured the displacement of single titin molecules in intact myofibrils at physiological sarcomere lengths (SLs). We used fluorescence microscopy combined with titin-specific quantum dot (Qdot) labels to track the length of the proximal tandem immunoglobulin (Ig) region of titin in stretched myofibrils. Our results demonstrate that proximal Ig domains undergo stepwise unfolding and refolding in situ, within the working range of the sarcomere. We further show that folding of a single proximal Ig domain of titin can deliver up to 105 zJ of elastic energy at 7.9 pN of force, which is more than the contractile energy supplied by the power stroke of a myosin motor (Piazzesi et al., 2007). We conclude that passive stretching of muscle tissue stores elastic energy by unfolding Ig domains and that refolding of these domains supplies an important, hitherto unrecognized, component of the force delivered by a contracting muscle.

RESULTS

Proximal Ig Region of Titin Undergoes Stepwise Changes in Length

To measure the dynamics of single titin molecules in intact sarcomeres, we isolated single myofibrils from rabbit psoas

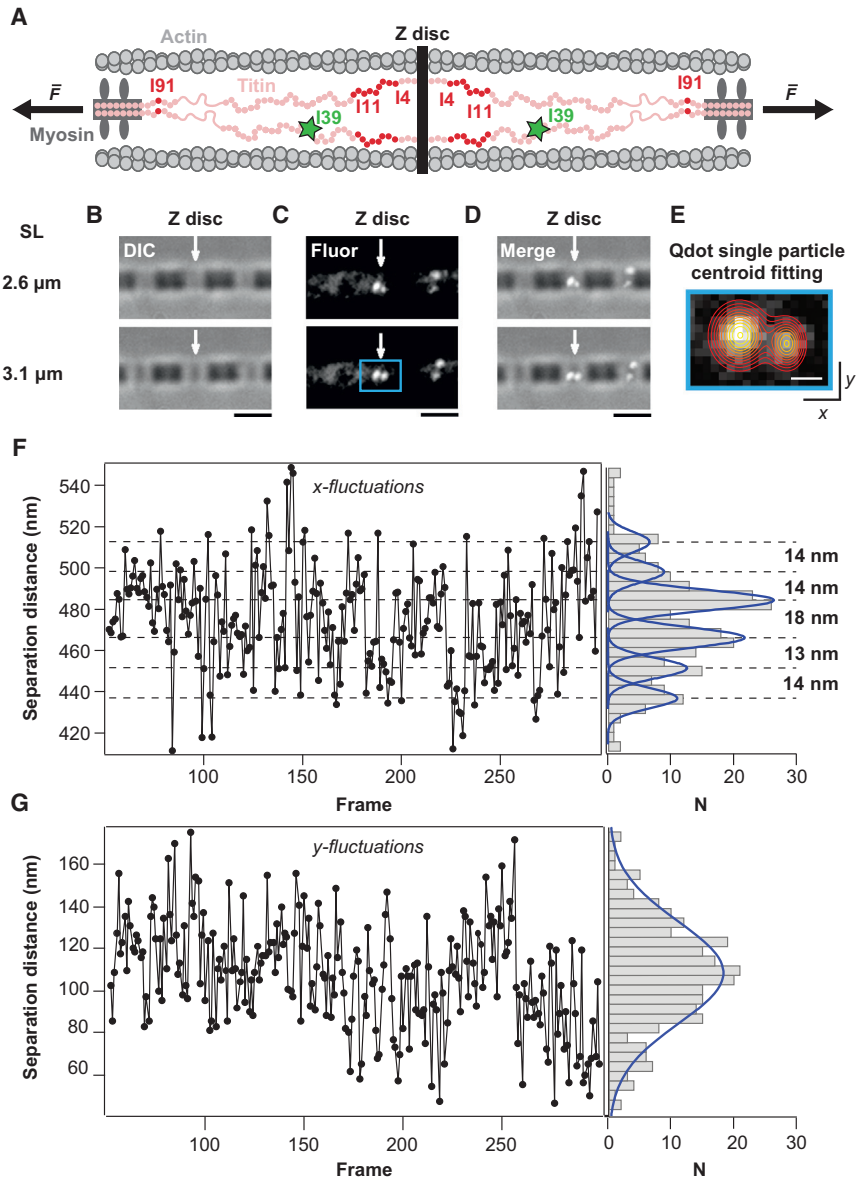

Figure 1. Single-Molecule Tracking in a Stretched Myofibril Reveals Discrete Extension States

(A) Schematic of the sarcomeric I-band.

(B) Single rabbit psoas myofibril stretched between two glass microneedles and shown at two SLs (2.6 μm in upper panel and 3.1 μm in lower panel).

(C) Fluorescence imaging of I39-specific Qdot labels shown in (A); same view as in (B).

(D) Merged view including (B) and (C). Pairs of Qdots are visible, spaced symmetrically around a Z-disc.

(E) Magnified view of the area highlighted in (C), showing an individual fit used to track the Qdot positions.

(F and G) Separation distance for individual Qdot pairs along the axis of applied force (F) and in the perpendicular direction (G). Right panels: histograms of separation distances. Qdots were tracked at ten frames per second.

Scale bars, 2 μm in (B)–(D) and 300 nm in (E).

muscles and attached them between two microneedles in an inverted light microscope. The SL of the myofibril was adjusted by changing the position of one of these needles using a piezoelectric stage. Sarcomeres were identified by differential interference contrast (DIC) microscopy (Figure 1B). Individual titin molecules were labeled in situ using antibody-conjugated Qdots targeted toward Ig domain I39 in the proximal Ig region (Figure 1A). At high labeling density, two closely spaced fluorescent stripes could be seen symmetrically around each Z-disc, verifying the specificity of the I39 antibodies (Figure S1). At low labeling density, individual Qdots could be detected in the myofibrillar I-bands. Qdot pairs (hereinafter referred to as doublets) were occasionally seen under these low labeling density conditions, spaced equidistantly around a Z-disc and, thus, likely marking two epitopes in adjoining sarcomeres (Figures 1C and 1D). Along the myofibrillar axis, two such epitopes are separated only by the Z-disc and proximal Ig domains, without any major flexible linkers in between (Figure 1A). Since the Z-disc behaves as a rigid object at low forces (Luther, 2009), we speculated that it would be possible to directly detect folding/unfolding of Ig domains by measuring the separation distance between the doublets. We tracked the Qdot separation distance along the axis of applied force using a centroid-fitting algorithm (Figure 1E; see Experimental Procedures).

When stretching the sarcomere to physiological extensions such as 3.1 μm (Lieber et al., 1994; Llewellyn et al., 2008; Wang et al., 1991), we observed that the Qdot doublets jumped along a discrete distribution of distances, as shown by the accumulated length histograms (Figure 1F, right panel). Similar results were found for several Qdot doublets in separate myofibrils, showing that the result is reproducible (Figure S2). A multipeak fixed-width Gaussian fit to the data revealed two independent populations of separation distances centered at 13 ± 3 nm and 22 ± 3 nm (Figures S2 and S3C). The y-fluctuations measured for the same Qdot doublets did not show discrete populations in the accumulated histograms (Figure 1G; Figure S2). Here, the fluctuations are larger in the x-direction than perpendicular to it, suggesting force-driven transitions within the titin molecules along the pulling coordinate (Figure S4). These measurements, therefore, indicate that the end-to-end distance of the proximal Ig region of titin undergoes discrete changes in length at an SL of 3.1 μm. These steps and the lack of a flexible unstructured segment between the Z-disc and domain I39 suggest that Ig domains from the proximal Ig region undergo stepwise unfolding-refolding transitions.

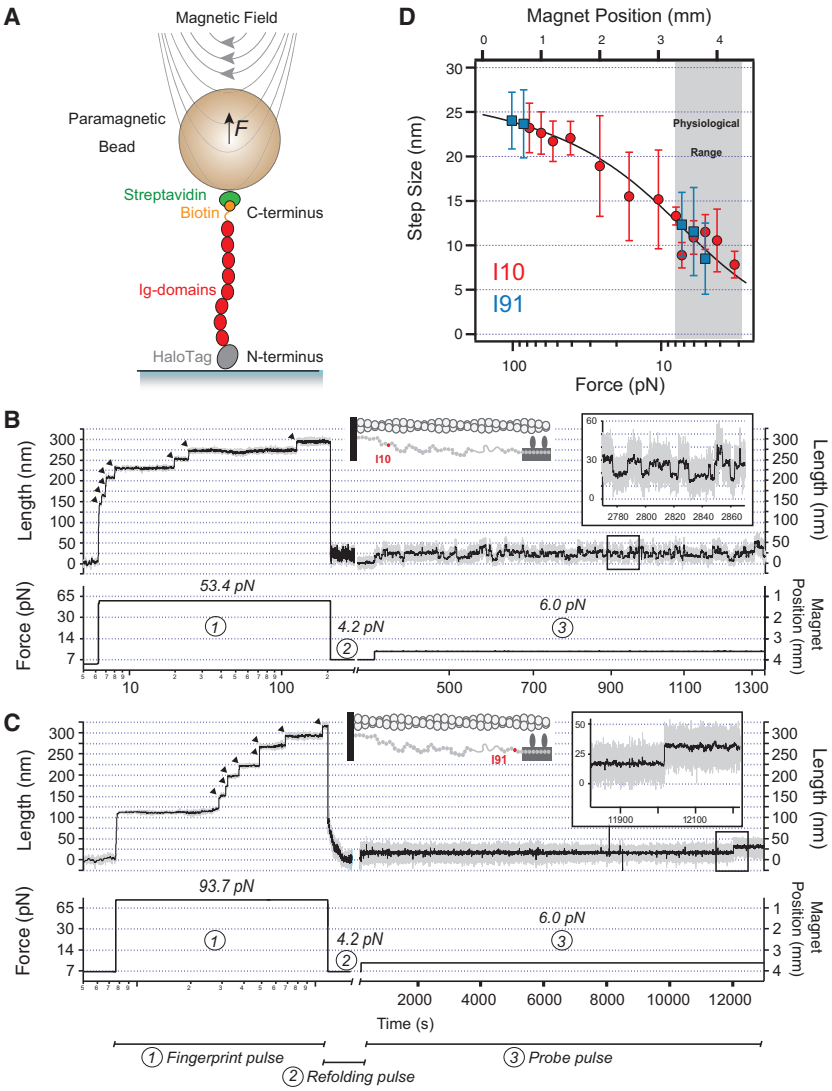

Figure 2. Dynamics of Ig Domains I10 and I91 at Physiological Forces

(A) Schematics of the magnetic-tweezers experiment showing a polyprotein tethered between a glass coverslip and a magnetic bead. Force is applied by varying the separation between a pair of permanent magnets and the magnetic bead.

(B and C) Dynamics of I10 (B) and I91 (C) (also known as I27) polyproteins under force; first fully unfolded by a fingerprint pulse (1), followed by a refolding pulse at low force (2), and then examined by a probe pulse (3). (Insets: positions of I10 and I91 in the half sarcomere and zoom-in of folding/unfolding events.) Arrowheads mark Ig domain unfolding events.

(D) Measured step sizes for I10 (red symbols) and I91 (blue symbols) are well fit by Equation S3 (solid black line). Data include both unfolding steps and refolding steps pooled together. The error bars represent SD. The experiments were recorded at ~260 fps and then smoothed.

See also Equation S3.

Earlier studies have inferred the force on single titin molecules from measurements of the passive SL-tension relationship for single myofibrils and from estimates of the number of parallel titin molecules per myofibrillar cross-sectional area. Accordingly, from 2.1- to 3.1-μm SL, the force per titin grows from <1 pN to 6–8 pN, assuming six titin molecules per half thick filament (Linke et al., 1998). Therefore, the in situ measurements of ~13- and ~22-nm steps are predicted to arise from the folding/unfolding reactions of the proximal Ig domains at 6–8 pN.

Titin Ig Domains Unfold and Refold in a Stepwise Manner at Physiological Forces

In order to test these predictions, we studied the behavior of isolated titin molecules using single-molecule force spectroscopy techniques. We combined magnetic-tweezers force spectroscopy (Chen et al., 2015; Liu et al., 2009; Yao et al., 2014) with HaloTag anchoring (Popa et al., 2013), allowing us to record the extension of Ig domains for several hours at nanometer resolution in passive force-clamp mode (Figure 2A). We selected two well-characterized titin Ig domains from the proximal and distal regions of human titin, I10 and I91 (Anderson et al., 2013; Li et al., 2002), to measure their dynamics and folding/unfolding steps over a wide force range. Both proteins were engineered as polyproteins containing eight repeats of the Ig domain, flanked at the N terminus by a HaloTag and at the C terminus by an AviTag (Figure 2A). The polyprotein constructs were covalently linked to a glass coverslip functionalized with HaloTag ligand (Popa et al., 2013) and to a magnetic bead coated with streptavidin. The polyproteins were exposed to forces varying between 3 and 100 pN by manipulation of a pair of permanent magnets positioned above the fluid cell.

Exposing these protein constructs to a high force caused the rapid unfolding of individual domains, which manifested as stepwise increases in the measured length (Figures 2B and 2C). In agreement with previous reports (Li et al., 2002), the I91 domain from the distal region was more mechanically stable than the proximal Ig domain I10, requiring higher pulling forces to unfold at a rate comparable to that of I10 (92.7 pN versus 53.7 pN; Figures 2B and 2C). More to the point, after allowing for complete refolding at 4.2 pN, pulling up to 6.0 pN showed these differences more starkly. In the example shown in Figure 2, at 6.0 pN, I10 underwent 202 stepwise unfolding/collapse events over a period of 23 min (Figure 2B). By contrast, at the same force, only one unfolding event was recorded for I91 over a 4-hr-long recording (Figure 2C). Notwithstanding their differing mechanical stability, both proteins showed step sizes that varied steeply with the pulling force (Figure 2D, I10 indicated by red circles and I91 indicated by blue squares). At the same force, unfolding and collapse step sizes were identical (Figures 2D and S5). Using similar pulse protocols, we collected a large number

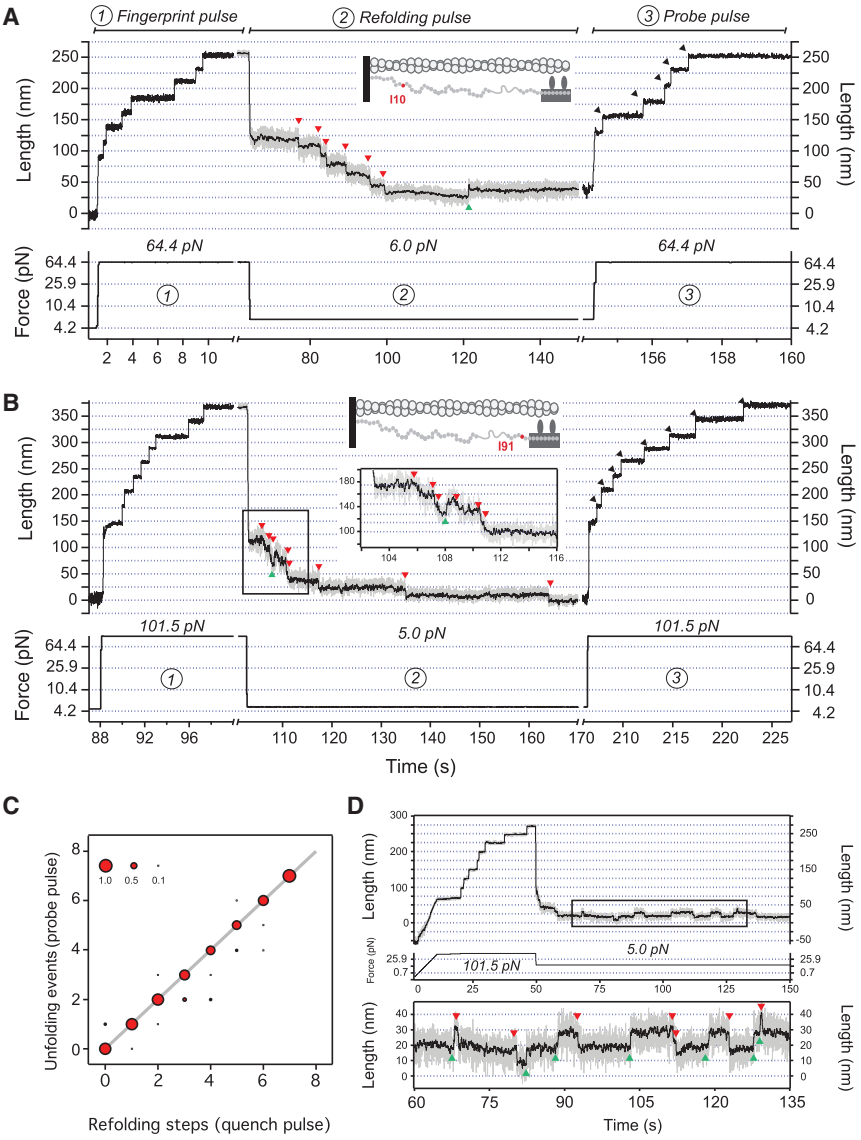

Figure 3. Titin Ig Domains from the Distal and Proximal Regions Refold in a Stepwise Manner

(A) Seven I10 domains are unfolded at high forces. Reducing the force to 6 pN results in the sequential folding of each of six domains indicated by 11-nm steps downward (red arrows). At this force, a single upward step (green arrow) indicates one of the folded domains again unfolding. A subsequent high-force probe pulse shows that five domains have acquired their native fold.

(B) I91 domains exhibit equivalent folding dynamics at 5 pN: three domains fold first, followed by unfolding and refolding of a single domain, and then folding of the remaining five domains. The subsequent high-force probe pulse shows that all eight domains have acquired their native fold.

(C) Downward steps at low force are highly correlated with unfolding steps in the subsequent probe pulse, indicating that the native fold is acquired after the Ig domain collapses.

(D) I91 domains proceed through a molten globule intermediate before acquiring their native folded structure. Contrasted with the slow unfolding dynamics of I91 in the folded state (Figure 2C), the I91 molten globule has low stability and is highly extensible. The I91 molten globule is easily unfolded (green arrows) at 5 pN and, therefore, contributes to the elasticity of titin.

of unfolding/collapse steps for both proteins over a range of 3–100 pN (Figure 2D). By combining our magnetic-tweezers magnet law (Supplemental Notes, Equation S1) with the worm-like chain (WLC) model of polymer elasticity (Supplemental Notes, Equation S2), we derived an expression (Supplemental Notes, Equation S3) that was readily fit to the measured step sizes versus magnet position (MP; Figure 2D). A fit of Equation S3 to the data gave values of 27.8 nm for the contour length (L_C) and 0.55 nm for the persistence length (p) (solid line in Figures 2D and S6B).

Ig Domains Collapse to a Highly Compliant Common State

After unfolding all eight Ig domains at a high force, quenching the force always resulted in a fast recoil, as the extended polypeptide adjusted to the new pulling force. At forces below 10 pN, this recoil was followed by a series of downward steps that we interpret as folding events. In contrast to the large differences observed in the rates of unfolding, the rate of descent of the folding steps was similar for both the I10 and I91 domains (Figures 3A and 3B). If these steps are associated with the folding of the Ig domains, one would expect the same number of unfolding events during a subsequent high-force probe pulse (Figures 3A and 3B). For the majority of recordings, in which 0–8 downward steps were observed during the refolding pulse, there was a 1:1 relationship between the number of downward steps and the number of unfolding events (Figure 3C). However, in many cases, there were fewer unfolding events than downward steps, indicated by the points below the 1:1 curve (Figure 3C). This observation indicates that a downward step does not necessarily lead to a natively folded domain. Most likely, there is an intermediate state that precedes the mechanically stable native fold. This intermediate state corresponds to the molten globule state that was observed before for Ig domain folding under force (Garcia-Manyes et al., 2009). The molten globule state shows low mechanical stability, readily converting back and forth from a collapsed state to the shorter molten globule state. The molten globule state is particularly apparent in the case of I91, which extended and collapsed rapidly to the molten globule state (Figure 3D), but required several hours to show even one unfolding event from a vastly more mechanically stable native state (Figure 2C). Although we expected I91 to rarely unfold and extend

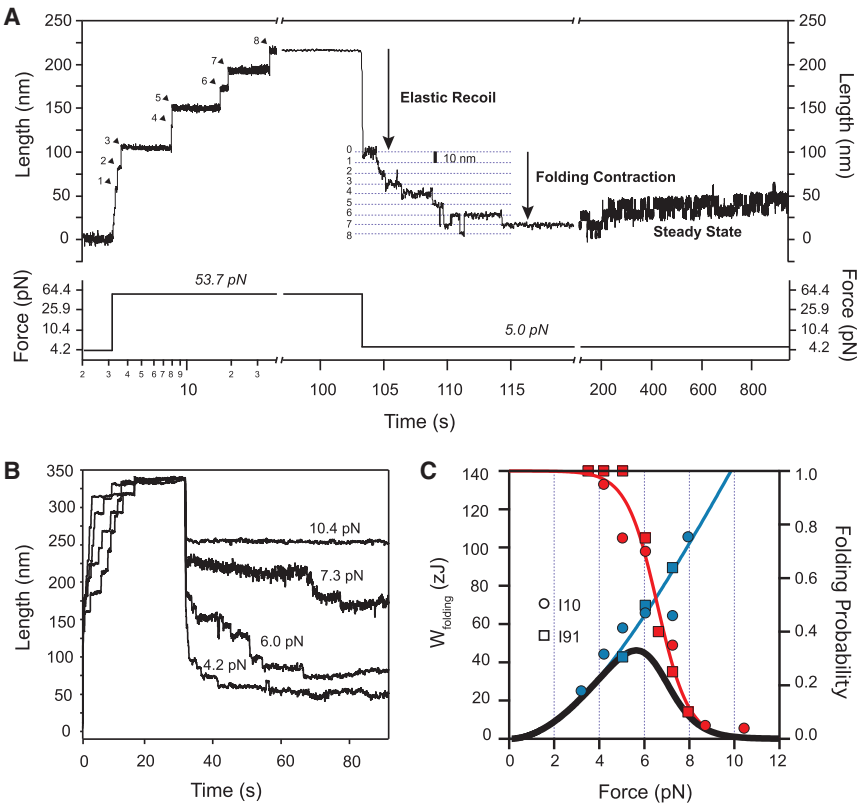

Figure 4. Titin Ig Domains Perform Mechanical Work during Folding

(A) When the stretching force is quenched, unfolded I10 domains shorten first with an elastic recoil, followed by a stepwise folding contraction.

(B) The folding contraction occurs over a narrow range of forces (4–10 pN).

(C) Folding work done by titin Ig domains (blue circles indicate I10, and squares indicate I91). The blue line is the work predicted by the WLC model (L_C = 27.8 nm; p = 0.55 nm). The folding probability measured at 60 s (red circles indicate I10, and squares indicate I91) is well described by a sigmoid (red line). The expected value of the energy delivered by folding (blue line × red line) peaks at 5.7 pN, delivering 46 zJ of contractile energy.

in vivo, we found that it repeatedly interconverted between the extended and molten globule states at low forces (<10 pN) as long as it did not acquire the native state (Figure 3D).

Intact Myofibril and Single-Molecule Measurements Match at 6 pN

Our in situ measurements showed that, at 6–8 pN of force, the proximal Ig region of titin underwent step changes in length of 13 ± 3 nm and 22 ± 3 nm (Figure S3). Our single-molecule studies with isolated I10 and I91 domains showed that 13 ± 3 nm steps occurred in the 5–12 pN range, in good agreement with our in situ measurements. However, we also observed much larger steps (22 ± 3 nm) in the single-myofibril QDot experiments (Figures 1F and S2), which could not be explained by the step sizes observed in the single-molecule experiments with I10 and I91. We reasoned that perhaps this mechanical behavior was unique to the native sequence of titin. To test this hypothesis, we cloned the segment of titin spanning Ig domains I4 through I11 (Figure 1A), which is contained within the proximal Ig region and was, therefore, tracked with our QDot experiments. Given the heterogeneous mechanical stability of the Ig domains present in this native segment (Li et al., 2002), we used a force-ramp protocol to unfold the individual Ig domains (Figure S3A). After unfolding the I4–I11 domains, the force was quenched for about 100 s to allow the domains to refold. The force was then increased to 6 pN and held constant for several minutes (Figures S3A and S7). At 6 pN, we readily observed mixed folding and unfolding steps that were similar in size to those observed in situ. Higher forces rapidly shifted the balance toward unfolding, making the observation of folding steps difficult. At 6.0 pN, I4–I11 showed numerous unfolding/refolding steps on a timescale of seconds (Figures S3B and S7). Hundreds of such stepwise transitions were recorded from several molecules (n = 5 molecules). Figure S3C compares histograms of the folding/unfolding step sizes collected in situ at an SL of 3.1 μm and from single I4–I11 molecules at 6.0 pN. Remarkably, the single-molecule force spectroscopy data showed two principal peaks centered at 10 ± 4 and 22 ± 5 nm, which are very similar to those measured in situ. Although the 22-nm steps observed in the single-myofibril data were originally thought to be due to the unfolding of two individual domains during the integration time of the camera, the force spectroscopy data suggested that these are distinct transitions (e.g., Figure S3B). Alternatively, it is unlikely that these steps are due to a calibration error, because several Qdot tracking experiments and several magnetic-tweezers experiments showed a mixture of both step sizes during the same recording. The high occurrence of these step sizes in I4–I11 is not surprising, given that this segment probably contains many endogenous interactions that are lost in the engineered homopolyproteins.

Stepwise Ig Domain Folding Provides a Large Amount of Elastic Energy to a Contracting Muscle

The remarkable agreement between the in situ and single-molecule data provides strong support for the view that folding/unfolding of titin Ig domains occurs in intact muscle tissue at physiological forces of 6–8 pN. Therefore, we examined in more detail the folding behavior of Ig domains in this force range. Figure 4A summarizes our single-molecule findings. Quenching the force down to 5.0 pN in a previously unfolded I10 polyprotein triggered first elastic recoil, followed by a stepwise folding contraction that eventually reached a steady state (Figure 4A). The stepwise folding contraction was found to be very sensitive to force. After unfolding all eight I10 domains at high force, the force was quenched to a value ranging from 4 to 10 pN (Figure 4B). Above

10 pN, no folding contraction was observed. Below 10 pN, the number of folding steps and their rate of appearance increased as the force was reduced. Reducing the force to 4 pN or less always resulted in complete refolding of all eight domains. From these data, we calculated the folding probability as a function of force for an unfolded I10 domain (Figure 4C, red circles). We did similar experiments with I91, which demonstrated nearly identical refolding probability over this range of forces (Figure 4C, red squares). For both domains, the transition from fully unfolded to fully folded was narrow. We fit a sigmoid to the folding probability data (Figure 4C, red curve), where the half point is at 6.6 pN and the 5%–95% range occurs over 4.1 pN. Therefore, reducing the load on titin by only a few piconewtons triggered the refolding of Ig domains, which is likely the case during active muscle contraction.

Owing to its force dependency (Figure 2D), a folding step can deliver varying amounts of elastic energy. We measured the amount of contractile work done by the folding of a single I10 or I91 domain, calculated as $F \cdot \Delta L$ (Figure 4C, blue squares indicate I10, and blue circles indicate I91). We showed that the force dependency of the folding step size closely follows the WLC model of polymer elasticity (Figure 2D). We used this model to fit the data of Figure 4C, calculated as $F_{WLC} \cdot \Delta L$ (Figure 4C, blue line). Folding steps that occur at higher forces are also larger (Figure 2D) and, hence, do more work and recover more energy (e.g., 105 zJ at 7.9 pN; Figure 4C). However, at higher forces, there is a lower probability of folding (Figure 4C, red curve). A more useful measure for evaluating the delivery of elastic folding energy in a contracting muscle is to compute the expected value of the work performed by a single titin Ig domain, calculated as the product of the work performed and the probability of folding (Figure 4C, black curve). We conclude that, for muscle to recover the maximum amount of elastic potential energy from Ig domain folding (peak expected value, 46 zJ), the force on titin during an extension/contraction cycle should vary between 8.6 pN (5% folding) and 5.7 pN (peak of the expected value function).

DISCUSSION

Muscle tissue derives its properties directly from the dynamics of its single molecules. In a muscle fiber, there are $\sim 2.4 \times 10^9$ titin molecules per square millimeter operating in parallel and acting independently of each other to provide elastic recoil to the sarcomere (Higuchi et al., 1993). Intimately connected to titin is the thick filament from which myosin heads protrude to interact with actin filaments in a Ca^{2+}- and ATP-dependent manner. These two molecular systems have been thought to operate independently from one another, with titin playing a role only during the passive extension of muscle and the myosin motors acting as the sole source of mechanical force during a contraction. In this paper, we provide evidence to support the view that the titin and myosin molecular systems both work together, over a narrow range of forces, to store and recover elastic mechanical energy from folding Ig domains during muscle contraction.

Our data demonstrate that unfolded proximal Ig domains can do a surprisingly large amount of contractile mechanical work. Indeed, we show that an unfolded I10 or I91 domain can deliver up to $W = 105$ zJ of contractile work at 7.9 pN (Figure 4C), which is nearly three times as much contractile work as that of a single myosin motor (~38 zJ; Piazzesi et al., 2007; Finer et al., 1994). However, folding steps are relatively rare at 7.9 pN of force, so a better measure of the recovery of elastic energy is its expected value, $E(W)$, which we calculate as the positive work done by the folding steps multiplied by their probability of occurrence (see Supplemental Notes). Thus, by dropping the force per titin down to 5.7 pN at the peak of the $E(W)$ distribution, a large number of folding Ig domains would be expected to deliver ~46 zJ per folding domain of contractile mechanical work. These calculations were done based on the folding steps of isolated I10 and I91 modules, which were observed to be as large as 13 nm at 8 pN (Figures 2 and 3). However, the folding steps measured in situ, as well as those measured from the native I4–I11 tandem Ig region, both showed steps found to be almost twice as big (~22 nm), producing ~132 zJ of contractile mechanical work at an operating force of 6 pN (Figures 4 and S3). Although the origin of the larger steps remains speculative, their high frequency of occurrence suggests that, in native titin, there are additional mechanisms in place to increase the delivery of elastic energy during Ig domain folding. It also appears that the measured Ig domain folding probability curve is a generic property of all unfolded domains. We chose to compare I10 and I91, from the proximal and distal regions of titin, as two well-studied extremes in mechanical stability. While the native state of I91 is significantly more stable (Figure 2), both domains demonstrate the same folding probability as a function of force. This result implies that recruitment of Ig domain unfolding will be complex and time dependent, whereas the contractile delivery of the folding energy will occur in synchrony and exactly over the same range of forces for all unfolded domains. If titin has unfolded a few of its Ig domains at a stretched length prior to the contraction, then the extra "kick" from titin folding should have a significant function in supporting muscle contraction.

For simplicity, we consider the case where there may be one myosin motor cycling while attached to a single titin molecule composed solely of tandem Ig domains (Figure 5A). In the extension phase of a relaxed sarcomere (low Ca^{2+}), the myosin head is disengaged from actin, and the load of 10 pN is transmitted directly to the titin molecule, triggering the unfolding and extension of an Ig domain (Figures 5A and 5B). Upon elevation of intracellular Ca^{2+}, the myosin head engages the actin filament, generating a force of 4 pN during the power stroke. This force is immediately subtracted from the force on the titin molecule, so that titin now experiences a stretching force of 6 pN, where the probability of folding is high. Folding of a single domain at 6 pN takes place in steps of ~10 nm; therefore, the folding energy delivered would be 60 zJ, which is larger than the energy delivered by the motor itself. The coincident force ranges over which both the motors and titin folding operate, as well as the distance over which folding Ig domains and myosin travel, are striking. Earlier studies had shown that the power stroke of a single myosin motor can generate forces ranging from 3 to 7 pN (Finer et al., 1994), whereas more recent data show that, in vivo, the force of an active myosin motor remains closer to 6 pN (Piazzesi et al., 2007). These forces are sufficient to fully straddle the folding probability curve of titin Ig domains where a 4-pN reduction in the stretching force increases the folding probability from

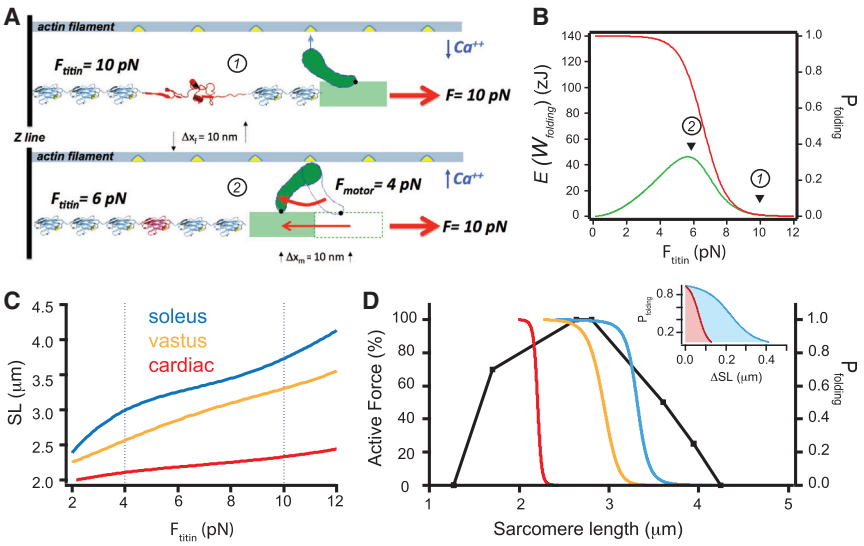

Figure 5. Mechanical Energy Delivered by a Folding Contraction Occurs at an Optimal SL that Is Muscle Type Specific

(A) Oversimplified sarcomere consisting of a single myosin motor and a single titin molecule. A relaxed sarcomere is stretched by 10 pN, unfolding an Ig domain, which extends by >13 nm (top; 1). Upon activation, the myosin head engages actin, and the resulting power stroke generates 4 pN of force, reducing the load on titin from 10 pN down to 6 pN, at which force the previously unfolded Ig domain will fold in a single 10-nm step, generating 60 zJ in contractile elastic energy (bottom; 2). Note that both folding and the power stroke shorten with matching step sizes (10 nm).

(B) Folding probability (red) and contractile elastic energy (green) shown in relation to the conditions (1 and 2) in (A).

(C) SL versus force relationships for titin measured from three types of human muscles—soleus, vastus lateralis, and cardiac—and using a value of 2.4 × 10^9 titin molecules per square millimeter of cross-sectional area (solid lines are fits to the experimental data from Kötter et al., 2014; Olsson et al., 2006; and Trombitás et al., 2003).

(D) Plot of Ig domain folding probability as a function of SL calculated using the measured Ig domain folding probability and the three relationships between SL and force shown in (C). The calculated range of SLs that are optimal for delivering a maximum amount of folding energy closely matches the peak of the (human) active force-length relationship (black line). The inset shows that cardiac muscle only needs to extend about 100 nm per sarcomere to fully straddle the Ig domain folding probability (5%–95%). By contrast, the much softer soleus muscle needs to extend by about 500 nm per sarcomere to cover a similar range of forces.

5% up to 95% (Figure 4C). To place the single-molecule folding data in perspective, we calculate that the mechanism shown in Figure 5A would readily lift an ~6-kg load (e.g., human vastus lateralis muscle, ~2,500 mm^2, 2.4 × 10^9 titin molecules per square millimeter) (Beneke et al., 1991; Higuchi et al., 1993), whereas the force generated by the motor alone could lift less than half that weight (see Supplemental Note 3).

A directly measurable parameter in striated muscle is SL. Many studies on isolated muscles have confirmed the close relationship between SL and the maximal amount of force generated during tetanus. These active (isometric) force-length relationships have been found to remain constant among many different types of muscles, in support of the sliding filament hypothesis. Human muscles develop a maximal force around 2.8 μm SL. Cardiac muscles operate on the ascending limb of the force-length relationship, whereas the soleus operates on the descending limb. These two muscles represent the extremes of muscle stiffness and express both the shortest and longest human titin isoforms, respectively. For each of these muscles, the relationship between passive tension and SL has been measured (Kötter et al., 2014; Trombitás et al., 2003). The relationship between force per titin molecule and SL for both cardiac muscle and the soleus is shown in Figure 5C. In addition, we also show data for the vastus lateralis, which falls somewhere in between (Olsson et al., 2006). The stiff cardiac muscle needs only to extend by remarkably little, from 2.1 μm up to 2.2 μm in SL, to double the force per titin from 4 pN to 8 pN. By contrast, the soleus needs a much larger extension from 2.9 μm to 3.4 μm to have the same effect. Therefore, it is clear that these two muscles will activate Ig domain folding in different regions of the active-force-versus-SL curve. We use the relationships shown in Figure 5C to plot the titin domain folding probability versus SL for all three muscle types. Figure 5D shows these results in relation to the active-force-versus-SL relationship for human muscles. It is remarkable that the titin folding probability curves are near the optimal SLs for all three types of muscles. The figure shows that the contribution that titin folding makes to muscle contraction is largest near the descending limb of the active length-tension relationship of skeletal muscles. In cardiac muscles, which have a much stiffer titin isoform, this contribution would support active contraction already on the ascending limb. Because skeletal muscle operates in vivo on the early descending limb of the active length-tension curve, whereas cardiac muscle operates on the ascending limb, the titin "kick" is largest within the physiological working range of either muscle type. It is also interesting to consider that the titin isoform present in the muscle tissue determines the relationship between force and SL (Figure 5C). Therefore, isoform switching will cause a shift in the position of the folding probability curve; most likely, in the operating range of SLs. Finally, the observation that only small SL changes are needed to fully activate the delivery of a titin folding contraction agrees well with direct measurements of SL changes during the full range of motion of a human limb (Llewellyn et al., 2008). From the evidence presented here, it appears inescapable that the folding of titin Ig domains generates a substantial component of the force in a contracting muscle. From this perspective, both the myosin motors and titin operate as an inextricable molecular system for the storage and delivery of mechanical energy.

EXPERIMENTAL PROCEDURES

For more details regarding the procedures used in this work, see the Supplemental Experimental Procedures.

Single Myofibril Mechanics

Single myofibrils were isolated from freshly excised rabbit psoas muscle as described previously (Linke et al., 1996). Experimental procedures were performed in accordance with the NIH Guide for the Care and Use of Laboratory Animals (8th ed.), published in 2011. All experimental protocols were approved by the Institutional Animal Care and Use Committee of Ruhr University Bochum. Single myofibrils were held for several seconds at or near slack SL and then were rapidly stretched (typically within 1 s) and held at the stretched SL for 10–30 s during data acquisition. When the myofibrils were released back to slack SL after the stretch, the slack SL was unchanged compared to before the stretch.

Single-Particle Tracking of Qdots

Single Qdot tracking was accomplished by simultaneously fitting two-dimensional (2D) Gaussian functions to pairs of Qdots for each frame. The separation distance between paired Qdots was calculated as the distance between the centroids of the Gaussian functions along the x axis. Multi-Gaussian fits to the histograms shown in Figure 1F and Figure S2 were carried out using the built-in multi-peak procedure in IGOR Pro.

Magnetic-Tweezers Experiments

The single-molecule experiments were carried out in fluid cells, where the bottom glass was functionalized with HaloTag (O4) amine ligand (Promega). Recombinant HaloTagged proteins immobilized on glass linked to paramagnetic streptavidin beads (Invitrogen) were pulled by changing the position of a pair of permanent magnets. The relationship between magnet position (MP) and force (F) is given by the equation $F(MP) = 65 \times e^{0.91(0.99-MP)}$ (see Equation S1 in Supplemental Information).

SUPPLEMENTAL INFORMATION

Supplemental Information includes Supplemental Experimental Procedures, seven figures, and Supplemental Notes and can be found with this article online at http://dx.doi.org/10.1016/j.celrep.2016.01.025.

AUTHOR CONTRIBUTIONS

J.M.F. and W.A.L. designed the project. P.K., W.A.L., and J.M.F. did the single-particle tracking experiments. J.A.R-P., E.C.E., I.P., and J.M.F. did the single-molecule magnetic-tweezers experiments. All authors wrote the paper.

ACKNOWLEDGMENTS

This work was supported by NIH grants GM116122 and HL061228 (J.M.F.), NSF grant DBI-1252857 (J.M.F.), and Deutsche Forschungsgemeinschaft grant SFB1002 (W.A.L.).

Received: March 20, 2015
Revised: September 30, 2015
Accepted: January 4, 2016
Published: February 4, 2016

REFERENCES

Anderson, B.R., Bogomolovas, J., Labeit, S., and Granzier, H. (2013). Single molecule force spectroscopy on titin implicates immunoglobulin domain stability as a cardiac disease mechanism. J. Biol. Chem. *288*, 5303–5315.

Beneke, R., Neuerburg, J., and Bohndorf, K. (1991). Muscle cross-section measurement by magnetic resonance imaging. Eur. J. Appl. Physiol. Occup. Physiol. *63*, 424–429.

Chen, H., Yuan, G., Winardhi, R.S., Yao, M., Popa, I., Fernandez, J.M., and Yan, J. (2015). Dynamics of equilibrium folding and unfolding transitions of titin immunoglobulin domain under constant forces. J. Am. Chem. Soc. *137*, 3540–3546.

Fernandez, J.M., and Li, H. (2004). Force-clamp spectroscopy monitors the folding trajectory of a single protein. Science *303*, 1674–1678.

Finer, J.T., Simmons, R.M., and Spudich, J.A. (1994). Single myosin molecule mechanics: piconewton forces and nanometre steps. Nature *368*, 113–119.

Garcia-Manyes, S., Dougan, L., Badilla, C.L., Brujic, J., and Fernández, J.M. (2009). Direct observation of an ensemble of stable collapsed states in the mechanical folding of ubiquitin. Proc. Natl. Acad. Sci. USA *106*, 10534–10539.

Granzier, H., and Labeit, S. (2002). Cardiac titin: an adjustable multi-functional spring. J. Physiol. *541*, 335–342.

Higuchi, H., Nakauchi, Y., Maruyama, K., and Fujime, S. (1993). Characterization of beta-connectin (titin 2) from striated muscle by dynamic light scattering. Biophys. J. *65*, 1906–1915.

Huxley, A.F., and Simmons, R.M. (1971). Proposed mechanism of force generation in striated muscle. Nature *233*, 533–538.

Kellermayer, M.S., Smith, S.B., Granzier, H.L., and Bustamante, C. (1997). Folding-unfolding transitions in single titin molecules characterized with laser tweezers. Science *276*, 1112–1116.

Kötter, S., Unger, A., Hamdani, N., Lang, P., Vorgerd, M., Nagel-Steger, L., and Linke, W.A. (2014). Human myocytes are protected from titin aggregation-induced stiffening by small heat shock proteins. J. Cell Biol. *204*, 187–202.

Li, H., Linke, W.A., Oberhauser, A.F., Carrion-Vazquez, M., Kerkvliet, J.G., Lu, H., Marszalek, P.E., and Fernandez, J.M. (2002). Reverse engineering of the giant muscle protein titin. Nature *418*, 998–1002.

Lieber, R.L., Loren, G.J., and Fridén, J. (1994). In vivo measurement of human wrist extensor muscle sarcomere length changes. J. Neurophysiol. *71*, 874–881.

Linke, W.A., and Fernandez, J.M. (2002). Cardiac titin: molecular basis of elasticity and cellular contribution to elastic and viscous stiffness components in myocardium. J. Muscle Res. Cell Motil. *23*, 483–497.

Linke, W.A., Ivemeyer, M., Olivieri, N., Kolmerer, B., Rüegg, J.C., and Labeit, S. (1996). Towards a molecular understanding of the elasticity of titin. J. Mol. Biol. *261*, 62–71.

Linke, W.A., Stockmeier, M.R., Ivemeyer, M., Hosser, H., and Mundel, P. (1998). Characterizing titin's I-band Ig domain region as an entropic spring. J. Cell Sci. *111*, 1567–1574.

Liu, R., Garcia-Manyes, S., Sarkar, A., Badilla, C.L., and Fernández, J.M. (2009). Mechanical characterization of protein L in the low-force regime by electromagnetic tweezers/evanescent nanometry. Biophys. J. *96*, 3810–3821.

Llewellyn, M.E., Barretto, R.P., Delp, S.L., and Schnitzer, M.J. (2008). Minimally invasive high-speed imaging of sarcomere contractile dynamics in mice and humans. Nature *454*, 784–788.

Luther, P.K. (2009). The vertebrate muscle Z-disc: sarcomere anchor for structure and signalling. J. Muscle Res. Cell Motil. *30*, 171–185.

Olsson, M.C., Krüger, M., Meyer, L.H., Ahnlund, L., Gransberg, L., Linke, W.A., and Larsson, L. (2006). Fibre type-specific increase in passive muscle tension in spinal cord-injured subjects with spasticity. J. Physiol. *577*, 339–352.

Piazzesi, G., Reconditi, M., Linari, M., Lucii, L., Bianco, P., Brunello, E., Decostre, V., Stewart, A., Gore, D.B., Irving, T.C., et al. (2007). Skeletal muscle performance determined by modulation of number of myosin motors rather than motor force or stroke size. Cell *131*, 784–795.

Piazzesi, G., Dolfi, M., Brunello, E., Fusi, L., Reconditi, M., Bianco, P., Linari, M., and Lombardi, V. (2014). The myofilament elasticity and its effect on kinetics of force generation by the myosin motor. Arch. Biochem. Biophys. *552-553*, 108–116.

Popa, I., Berkovich, R., Alegre-Cebollada, J., Badilla, C.L., Rivas-Pardo, J.A., Taniguchi, Y., Kawakami, M., and Fernandez, J.M. (2013). Nanomechanics of HaloTag tethers. J. Am. Chem. Soc. *135*, 12762–12771.

Rief, M., Gautel, M., Oesterhelt, F., Fernandez, J.M., and Gaub, H.E. (1997). Reversible unfolding of individual titin immunoglobulin domains by AFM. Science *276*, 1109–1112.

Trombitás, K., Wu, Y., McNabb, M., Greaser, M., Kellermayer, M.S., Labeit, S., and Granzier, H. (2003). Molecular basis of passive stress relaxation in human

soleus fibers: assessment of the role of immunoglobulin-like domain unfolding. Biophys. J. *85*, 3142–3153.

Tskhovrebova, L., and Trinick, J. (2003). Titin: properties and family relationships. Nat. Rev. Mol. Cell Biol. *4*, 679–689.

Tskhovrebova, L., Trinick, J., Sleep, J.A., and Simmons, R.M. (1997). Elasticity and unfolding of single molecules of the giant muscle protein titin. Nature *387*, 308–312.

Wang, K., McCarter, R., Wright, J., Beverly, J., and Ramirez-Mitchell, R. (1991). Regulation of skeletal muscle stiffness and elasticity by titin isoforms: a test of the segmental extension model of resting tension. Proc. Natl. Acad. Sci. USA *88*, 7101–7105.

Yao, M., Goult, B.T., Chen, H., Cong, P., Sheetz, M.P., and Yan, J. (2014). Mechanical activation of vinculin binding to talin locks talin in an unfolded conformation. Sci. Rep. *4*, 4610.

Cell Reports, Volume *14*

Supplemental Information

Work Done by Titin Protein Folding Assists Muscle Contraction

Jaime Andrés Rivas-Pardo, Edward C. Eckels, Ionel Popa, Pallav Kosuri, Wolfgang A. Linke, and Julio M. Fernández

SUPPLEMENTAL EXPERIMENTAL PROCEDURES

Single myofibril mechanics

Freshly isolated single myofibrils (Linke et al., 1996) were imaged by differential interference contrast microscopy (DIC) or by epifluorescence microscopy using a Zeiss Axiovert 135 inverted microscope. Movies were recorded with an Andor iXon EMCCD camera using Solis software (Andor Technology). In the pulling experiments, every myofibril (diameter ~1 µm) was picked up using two sharp glass microneedles (custom-pulled) coated at their tips with water curing silicone adhesive (mixture of Dow Corning RTV 3145 and 3140). Each microneedle was connected to a 3D piezo flexure stage (three P-280.30, Physik Instrumente) and precision 3D translation stage (UMR8A, Newport Corp). The experiments were performed at room temperature in relaxing solution (composition: 1 mM free Mg^{+2}, 100 mM KCl, 2 mM EGTA, 4 mM $Mg{\cdot}ATP^{-2}$ and 10 mM imidazole; pH 7.0) in the presence of 10 mM DTT (Sigma, Hamburg, Germany), which reduced Qdot blinking. To limit titin degradation all the solutions contained protease inhibitor leupeptin (4 µg/ml).

Immunofluorescence microscopy

Antibodies were used to attach Qdots to the proximal Ig domain I39 of titin (**Figure S1**). Single myofibrils were pre-stretched to 2.6 µm SL and labeled with the primary I39 antibody and then Qdot-conjugated anti-goat IgG (Q11441MP; Invitrogen; Odots emitting at 525 nm). After each incubation with the primary or secondary antibody, the sample was carefully washed at least three times with relaxing solution. The myofibril was returned to slack SL (2.1-2.3 µm) before starting the measurements. Fluorescence experiments were performed on a Zeiss Axiovert 135 microscope in epifluorescence mode (filterset XF301, Qdot525; Omega Optical) with a 100×, 1.4 NA oil immersion objective and a 2.5× magnifying lens. An Andor iXon EMCCD camera was used to acquire fluorescence data at 10 Hz, with an exposure time of 30-40 ms.

Single-particle tracking of Qdots

We used the piezoelectric stage to apply a step length increase to a tethered myofibril where a Qdot doublet could be clearly identified. In this extended state, we tracked the Qdot separation distance along the axis of applied force, using an EMCCD camera (iXon, Andor) and a centroid-fitting algorithm (**Figure 1E**). While the raw data showed no readily discernible transitions, discrete peaks were clearly visible when the observed separation distances were accumulated in a histogram (**Figure 1F**). The appearance of these peaks was not sensitive to binning parameters. Similar results were found for several Qdot doublets in separate myofibrils, showing that the result is reproducible (**Figure S2**). The effect was force-dependent, since discrete separation distance peaks were not seen along the axis perpendicular to the direction of applied force, or between Qdots on clean glass in the absence of force. Discrete peaks were furthermore not visible at frame rates below 10 Hz or when averaging subsequent frames, indicating that they arise from discrete states that interchange on the sub-second timescale.

Protein expression and purification

For the single-molecule experiments three different constructs were used. The native fragment I4-I11 from the proximal Ig region of titin was flanked by an N-terminal HaloTag enzyme (Los et al., 2008) and a C-terminal AviTag. Both terminal modifications allow manipulate single molecules in a very broad range of forces for very long period of time (Chen et al., 2015). The domains I10 and I91 were engineered in polyproteins with 8 repeats, flanked in N- and C-terminal with the HaloTag and AviTag, respectively. Both polyproteins, HaloTag-$(I10)_8$-AviTag and HaloTag-$(I91)_8$-AviTag, were employed to calibrate the force for the magnetic-tweezers experiments (**Figure 2B**). All the proteins were expressed and purified as described previously (Popa et al., 2013a).

Magnetic-tweezers experiments

Measurements were performed on an inverted microscope modified with a piezo objective positioner (P-721 and P-725 PIFOC, Physik Intrumente), a magnet positioner (LFA-2010, Equipment Solutions) and a high-speed camera (AVT Pike F-032B, Allied Vision Technologies). Fluid chambers, which were made by two cover slides separated by two strips of parafilm, contained the chemistry necessary to immobilize the HaloTag proteins (Popa et al., 2013b). Briefly, the bottom glass, after several washes, was silanized, modified with glutaraldehyde, and finally functionalized with HaloTag (O4) amine ligand. Amine polystyrene beads (Spherotech), which were used as a reference during the measurement, were covalent linked to the glass after the glutaraldehyde modification. Paramagnetic beads (Invitrogen) were tethered to the proteins using biotin-streptavidin linkage. All experiments were performed in 20 mM Tris-HCl pH 7.4, 2 mM $MgCl_2$, 150 mM NaCl and 1% BSA. All data acquisition and processing was performed in Wavemetrics Igor Pro.

.

SUPPLEMENTAL FIGURES

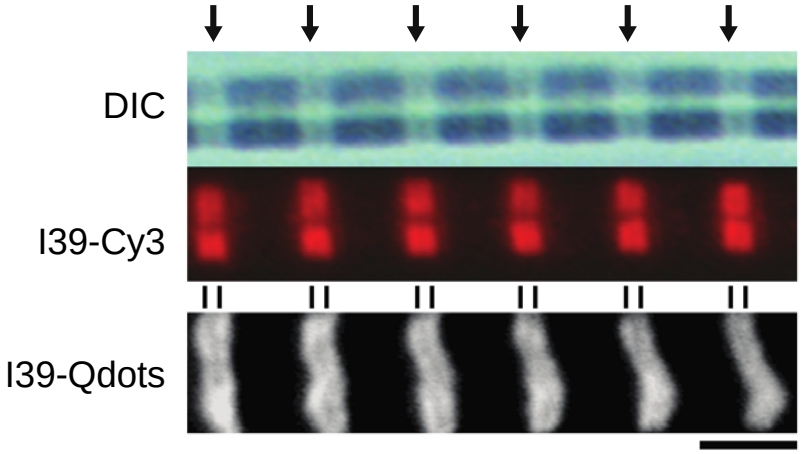

Figure S1. Regular I-band staining of titin I39 antibody epitope at high labeling density, related to Figure 1
Top: Rabbit psoas myofibril doublet imaged using DIC. Middle: Corresponding field of view in epifluorescence mode showing striated staining pattern obtained with titin I39 antibody and Cy3-conjugated secondary antibody. Bottom: Striated staining pattern obtained with I39 antibody and secondary antibody-conjugated Qdots. Double-banded stainings around the Z-disk indicate I-band position of titin epitope (vertical lines). Arrows, Z-disk region; Scale bar, 2 µm.

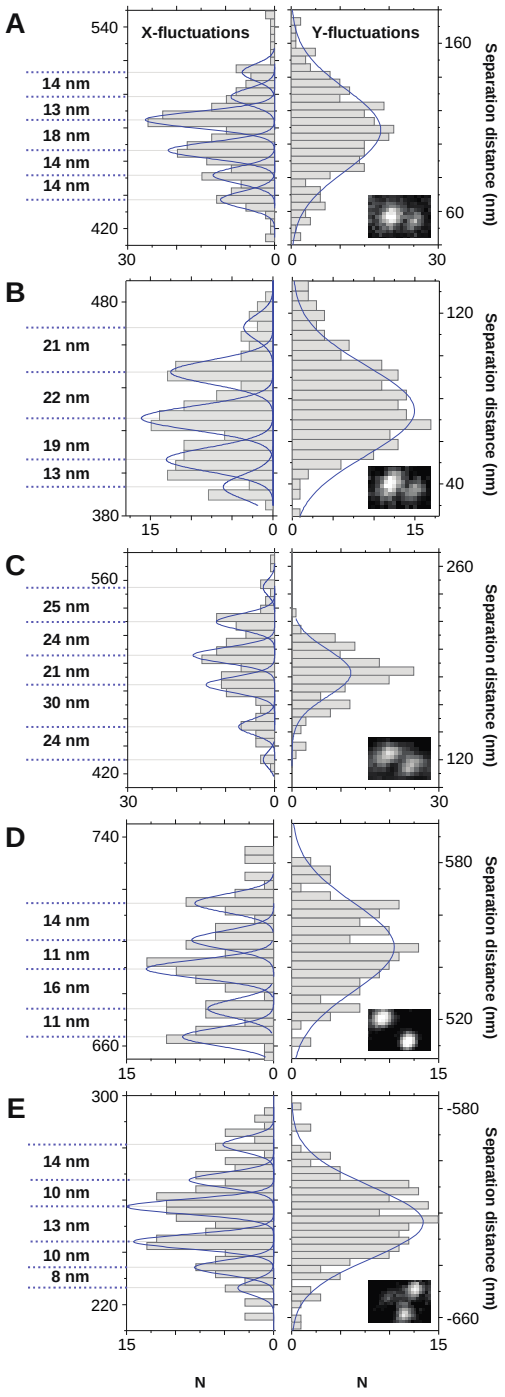

Figure S2. Binned separations of quantum dot pairs in the x- and y-directions, related to Figure 1
(A-E) Five pairs of quantum dots tracked during myofibril stretching exhibited motion in the x- and y-directions. Separation distances are binned and then fit with a fixed-width, multipeak fitting routine along the coordinate of pulling (x-direction). Motion perpendicular is collected into bins with the same width as x but does not show well-resolved Gaussian peaks. Insets show microscopy images of the quantum dot pairs.

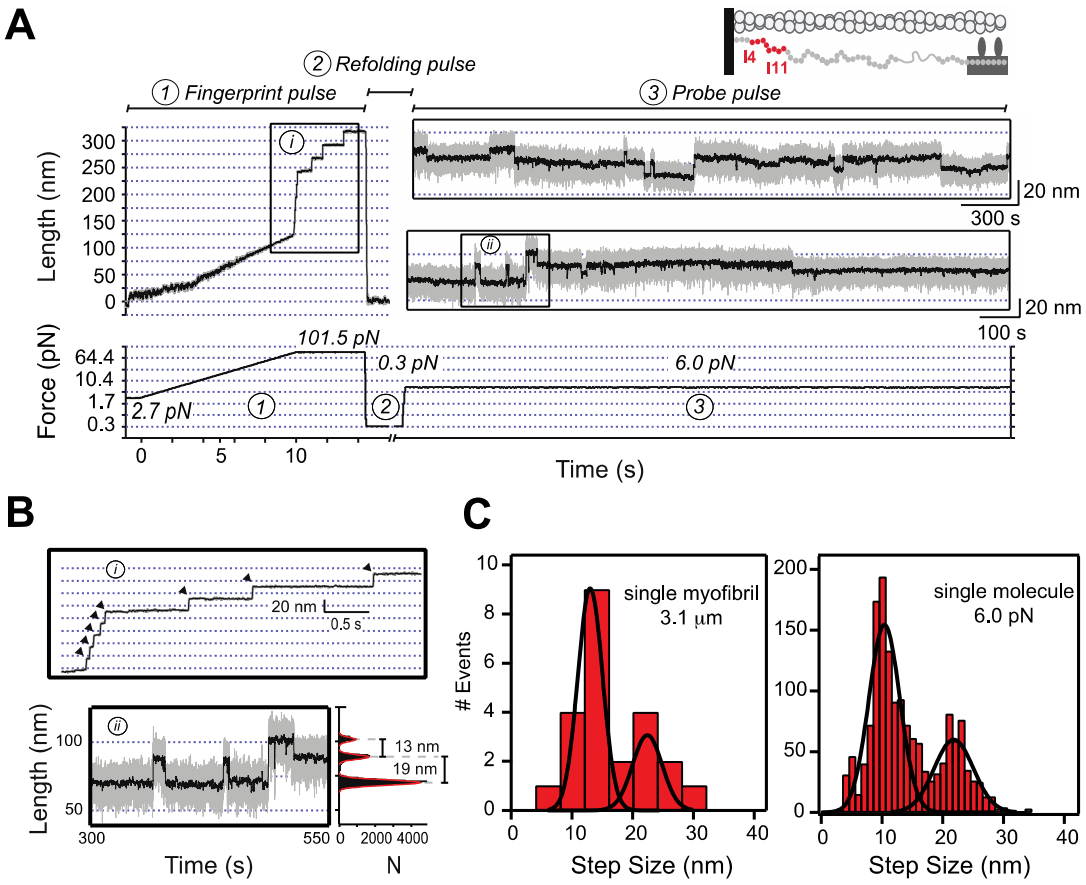

Figure S3. Single-molecule magnetic tweezers recording of an I4-I11 molecule at physiological forces, related to Figure 2

(A) Representative recording showing the dynamics of the native I4-I11 segment under force. A force-ramp between ~3 and ~100 pN was employed during the *fingerprint pulse*. The force was quenched to 0.3 pN to allow refolding for all the domains during the *refolding pulse*. During the *probe pulse*, forces below 10 pN were explored to simulate conditions experienced during the QDot experiments. In the figure, two representative recording are shown at 6.0 pN.

(**B**) Top: magnification unfolding steps from the trace in (A) during the *fingerprint pulse (i)*. Bottom: magnification of the unfolding-refolding transitions from the trace in (A) during the *probe pulse (ii)*. Histograms to the right measure the magnitude of the extension, demonstrating steps of both 13 and 19 nm in the same molecule.

(C) Cumulative histograms of all stepwise extension measured at the myofibril and single molecule level, respectively. Left: the separation between I39 doublets in titin from intact myofibrils under force (3.1 μm sarcomere length) shows discrete changes in distance with a spacing of 13 ± 3 and 22 ± 3 nm (n=5 independent measurements). Right: histogram of measured step sizes obtained from magnetic tweezers recordings from several (n=5) I4-I11 molecules exposed to 6.0 pN of force. Single molecule recording show two populations centered at 10 ± 4 and 22 ± 5 nm (n= 1557 events, 5 molecules). The experiments were recording at frame rates of ~260 Hz, then smoothed with a running average filter.

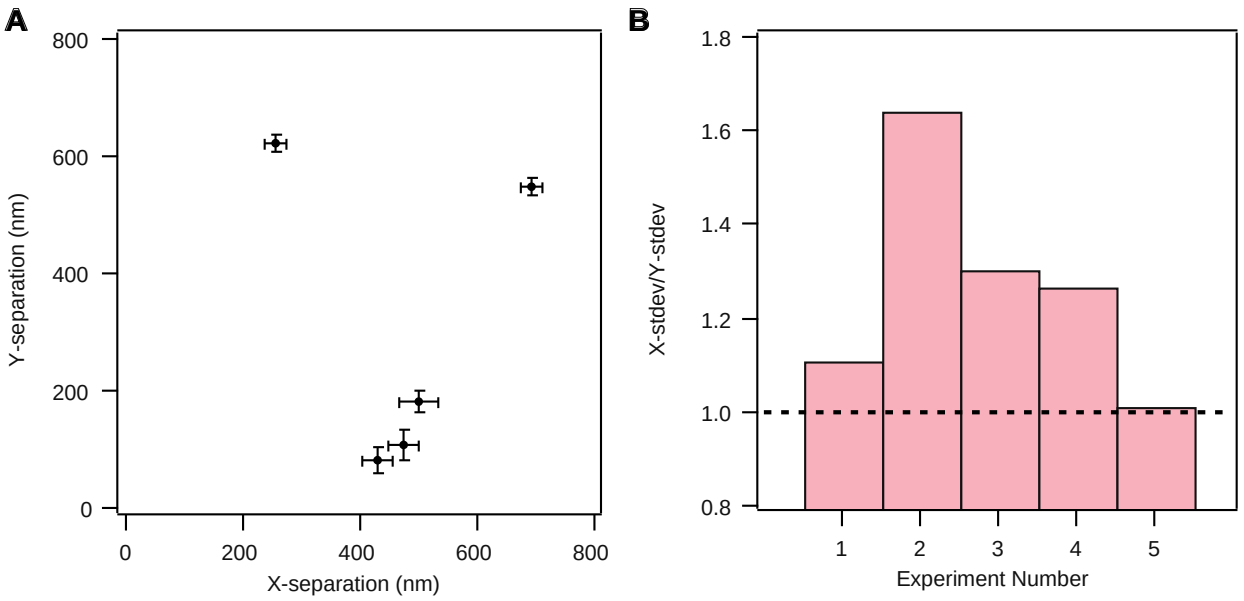

Figure S4: Anisotropy of quantum dot fluctuations, related to Figure 1
(A) Average separation distance for each of the five quantum dot pairs in the x- and y-directions. Error bars indicate the standard deviation of the separation distance. **(B)** Anisotropy of the qdot fluctuations can be seen by comparing the ratio of the standard deviations in the x- vs y-directions. All Qdot pairs show a ratio > 1.0, demonstrating that the myofibril architecture is deforming along the pulling axis.

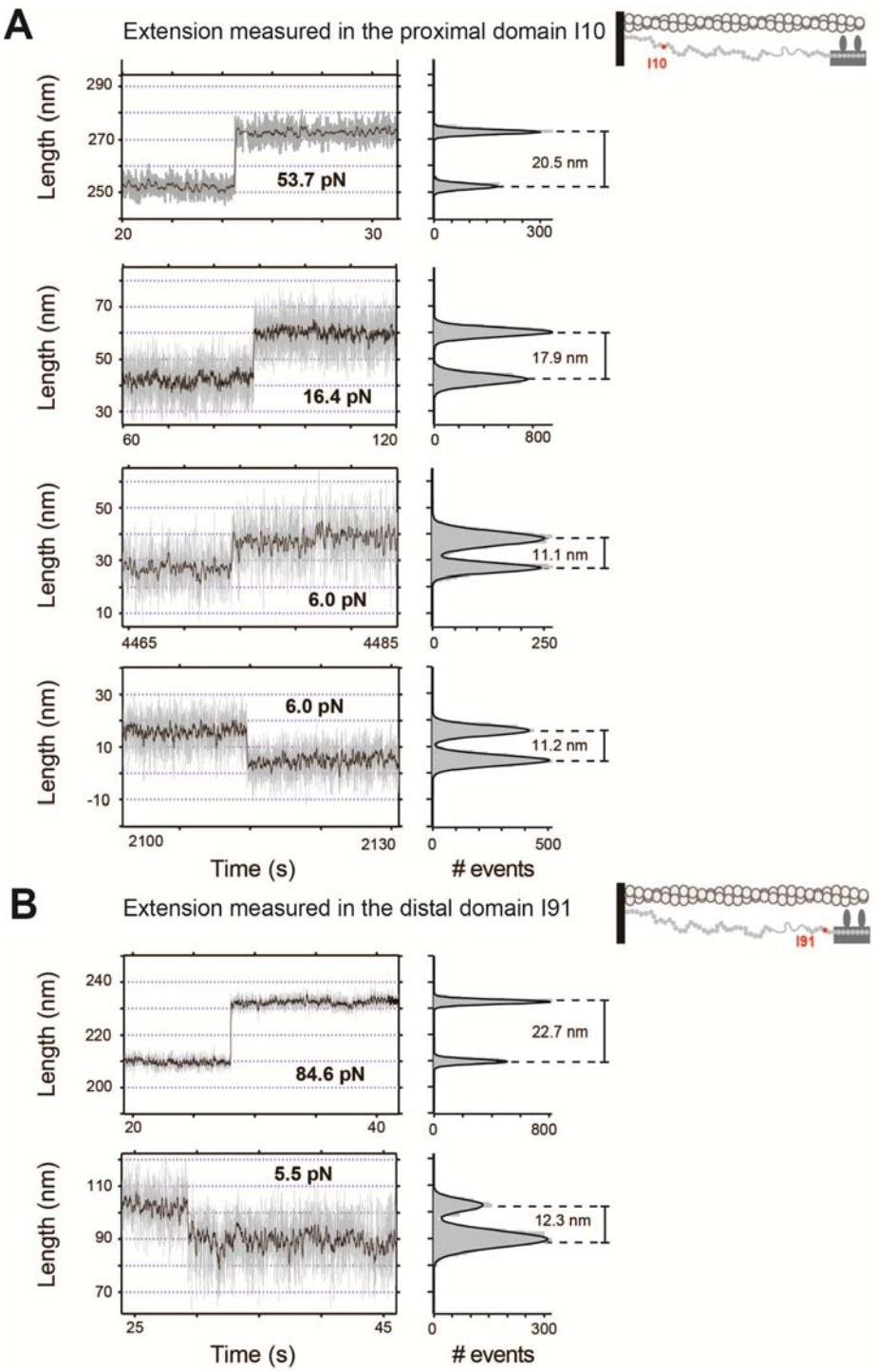

Figure S5. Force dependency of the unfolding-refolding steps, related to Figure 2
(A) and **(B)** Unfolding and refolding steps measured at different force, present in the proximal domain I10 and the distal domain I91, respectively.

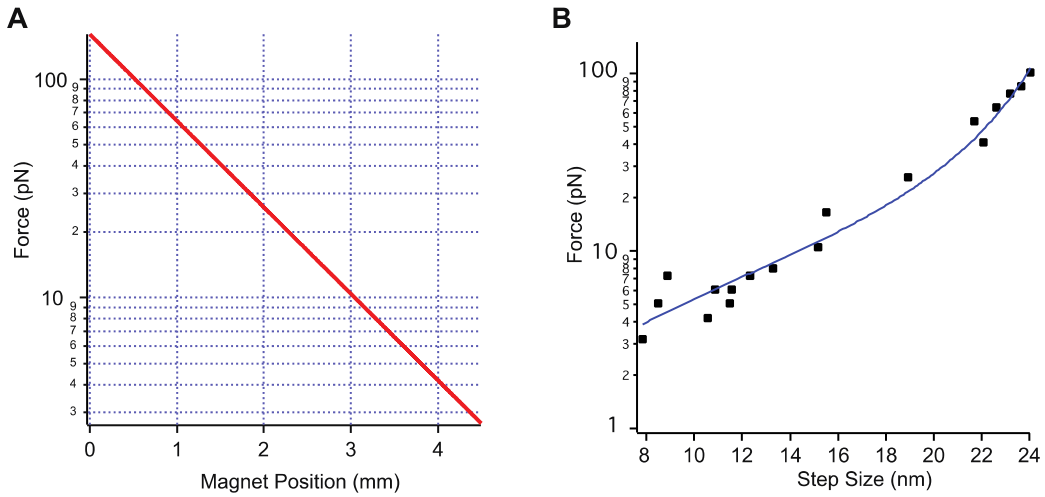

Figure S6. Magnet law of the tweezers instrument and fitting of the WLC model, related to Figure 2
(A) Magnet law for the experimental setup. The force exerted by the magnets depends on the magnet distance from the fluid chamber according to equation S1 (below). **(B)** The worm-like chain model of polymer elasticity fit to the experimentally measured step sizes in I10 and I91 provides a contour length L_C = 27.8 nm and a persistence length p = 0.55 nm.

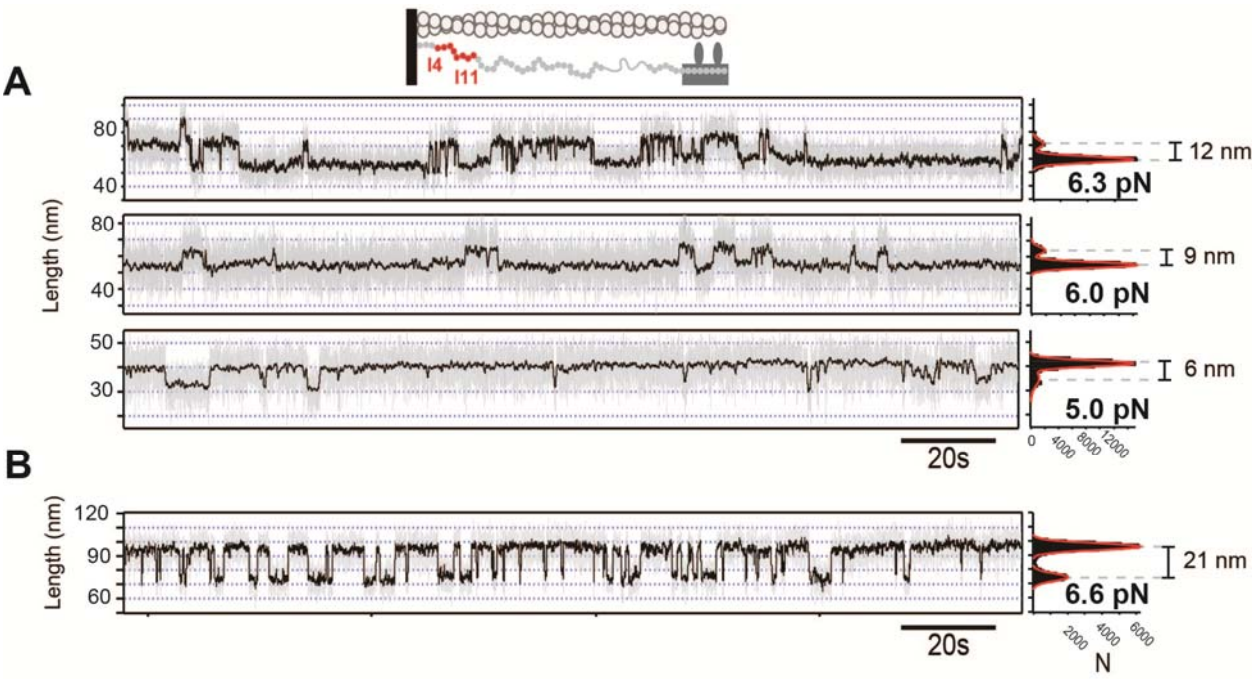

Figure S7. Dynamics of the I4-I11 segment at physiological forces, related to Figure 2 and 3
(A) I4-I11 at low forces shows the characteristics of single Ig domains unfolding and refolding, in the range between 6.3-5.0 pN. **(B)** Certain recordings demonstrate a step size not predicted by the WLC model. This step size is roughly twice the step size predicted at 6.6 pN and may be caused by inter-domain interactions or domain swapping. Bar in every recording corresponds to 20 s.

SUPPLEMENTAL NOTES

Note 1: *Measuring the polymer properties of an Ig domain (related to Experimental Methods)*

Calibration of the magnetic tweezers was performed using the B-S transition of a long DNA molecule combined with the force dependency of the step size of the B1 domain from Protein L (L_C = 18.6 nm and p = 0.58 nm). The resulting magnet law is well described by the following formula:

$$F(MP) = 65 \cdot e^{0.91(0.99-MP)} \quad \textbf{(Eq.S1)}$$

where F is the force in pN and MP is the measured magnet position in mm (**Figure S6A**, red line) (Popa et al, 2016). The contour length and persistence length of I10 were determined by fitting the step size to the WLC model of polymer elasticity:

$$F_{WLC}(x) = \frac{k_B T}{p}\left[\frac{1}{4}\left(1-\frac{x}{L_C}\right)^{-2} - \frac{1}{4} + \frac{x}{L_C}\right] \quad \textbf{(Eq.S2)}$$

Setting $F_{MP} = F_{WLC}$ allows us to solve for $MP(x)$ which are the two values measured in the experiments in Figure 2D:

$$MP(x) = 0.99 - \frac{\ln(F_{WLC}(x)/65)}{0.91} \quad \textbf{(Eq.S3)}$$

Fitting this equation to the data provides the parameters L_C = 27.8 nm and p = 0.55 nm (Figure 2D, black line). The resulting WLC model for $F_{WLC}(x)$ using these parameters is shown in **Figure S6B** (blue line) alongside the experimental data.

Note 2: *Calculation of work performed by protein folding (related to Figure 5)*

The work performed by a collapsing/folding Ig domain at constant force is calculated as $F \cdot x$, where x is the change in the end-to-end length of the protein upon collapsing/folding and F is the force calculated from the magnet law of the magnetic tweezers (**Eqn. S1**). Multiplying x (F) (**Figure 2D**, black line) by the force F (**Figure 2D**, abscissa) computes the work done by protein collapsing at any given force (**Figure 5C**, blue line).

Note 3: *Calculation of force generated by the vastus lateralis muscle group (related to Figure 5):*

$$2500\ mm^2 \cdot \frac{2.4 \cdot 10^9\ molecules}{mm^2} \cdot \frac{10\ pN}{molecule} \cdot \frac{N}{10^{12}\ pN} \cdot \frac{1}{9.81\ m \cdot s^{-2}} = 6\ kg$$

SUPPLEMENTAL REFERENCES

Chen, H., Yuan, G., Winardhi, R.S., Yao, M., Popa, I., Fernandez, J.M., and Yan, J. (2015). Dynamics of equilibrium folding and unfolding transitions of titin immunoglobulin domain under constant forces. Journal of the American Chemical Society *137*, 3540-3546.

Linke, W.A., Ivemeyer, M., Olivieri, N., Kolmerer, B., Ruegg, J.C., and Labeit, S. (1996). Towards a molecular understanding of the elasticity of titin. Journal of molecular biology *261*, 62-71.

Los, G.V., Encell, L.P., McDougall, M.G., Hartzell, D.D., Karassina, N., Zimprich, C., Wood, M.G., Learish, R., Ohana, R.F., Urh, M., *et al.* (2008). HaloTag: a novel protein labeling technology for cell imaging and protein analysis. ACS chemical biology *3*, 373-382.

Popa, I., Berkovich, R., Alegre-Cebollada, J., Badilla, C.L., Rivas-Pardo, J.A., Taniguchi, Y., Kawakami, M., and Fernandez, J.M. (2013a). Nanomechanics of HaloTag tethers. Journal of the American Chemical Society *135*, 12762-12771.

Popa, I., Kosuri, P., Alegre-Cebollada, J., Garcia-Manyes, S., and Fernandez, J.M. (2013b). Force dependency of biochemical reactions measured by single-molecule force-clamp spectroscopy. Nature protocols *8*, 1261-1276.

Popa, I, Rivas-Pardo, J.A., Eckels, E.C., Echelman, D., Valle-Orero, J. and Fernández, J.M (2016). A HaloTag Anchored Ruler for Weeks-Long Magnetic Tweezers Studies of Protein Dynamics. *Submitted*.